Article published online: 2024-08-21

Original Research Article

Characterisation of Aqueous Ultra-high Homeopathic Potencies: Nanoparticle Tracking Analysis

Michel Van Wassenhoven[1] Martine Goyens[2] Pierre Dorfman[3] Philippe Devos[4] Jean-Louis Demangeat[5]

[1] Coordinator of DynHom Research Project, Chastre, Belgium
[2] Pharmaceutical Association for Homeopathy, Wépion, Belgium
[3] M.R.C. Endowment Fund, Private Academy of Science™, Meyzieu, France
[4] Unio Homoeopathica Belgica, Evergem, Belgium
[5] Nuclear Medicine Department, General Hospital, Haguenau, France

Address for correspondence Michel Van Wassenhoven, MD, Chaussée de Bruxelles, 128 b5, B-1190 Brussels, Belgium (e-mail: michelvw@homeopathy.be).

Homeopathy

Abstract

Background and Objectives Over the past decade, research using various methods has claimed the material nature, including nanoparticles (NPs), of high homeopathic potencies. The current study aims to verify these findings using NP tracking analysis (NTA).

Methods Six independent serial dilutions of commonly used homeopathic medicines —either soluble (*Gelsemium*, *Pyrogenium*, *Kalium mur*) or insoluble (*Cuprum*, *Argentum*, *Silicea*)—were prepared according to European Pharmacopoeia standards. We compared the homeopathic dynamisations (DYNs) in pure water with their potentised controls and with simple dilutions (DIL) up to 30cH/10^{-60}. We also tested the influence of the container (glass or PET) on the solvent controls.

Results We observed the presence of particles from 20 to 300–400 nm in all DYNs, DILs and controls, except in pure unstirred water. The sizes and size distributions of NPs in high homeopathic potencies were smaller than those in controls for soluble sources and larger for insoluble sources, even above 11cH. The opposite behaviour was observed in the number of NPs. When comparing DYN and DIL, the number, size, presence of aggregates or chains and brightness of NPs increased with DYNs, which was also observed above 11cH. Many NPs scattered light of low intensity, indicating the presence of material particles. The container had a significant effect on the number and size of NPs, indicating the involvement of the atmosphere and leaching processes.

Conclusion Homeopathic medicines contain NPs with specific properties, even when diluted beyond Avogadro's number. Homeopathic potentisation is not a simple dilution. The starting material, the solvent used, the type of container and the manufacturing method influence the characteristics of these NPs. The nature of these NPs is not known, but most likely they are a mixture of nanobubbles and elements from the atmosphere and container, including insoluble ones.

Keywords
- nanoparticles
- nanobubbles
- homeopathic medicines
- ultra-high dilutions
- potentisation
- dynamisation
- nanoparticle tracking analysis

received
January 21, 2024
accepted after revision
May 2, 2024

DOI https://doi.org/10.1055/s-0044-1787782.
ISSN 1475-4916.

Georg Thieme Verlag KG, Rüdigerstraße 14, 70469 Stuttgart, Germany

Introduction

Homeopathy is a traditional form of medicine that has been used worldwide for more than 200 years. However, due to the theoretical absence of any molecule of the starting material in ultra-high dilutions above Avogadro's number, that is, 12cH, there is an increasing need for a clear explanation of the nature of these medicines. It is often ignored that the actual manufacturing process is more than simple dilution—it involves a stepwise potentisation (for water-soluble material), also called 'dilution and dynamisation', which is described in the European Pharmacopoeia.[1] For insoluble starting materials, the process requires two or three preliminary steps of grinding (trituration) in pure lactose. Although the recent literature on randomised controlled trials[2–4] supports a specific effect of homeopathic treatments, the debate about plausibility and evidence can only be resolved by basic research.[5]

Among the many physico-chemical techniques used for this purpose, nuclear magnetic resonance (NMR) has been recognised as one of the most promising and powerful tools,[6–8] demonstrating that liquid homeopathic medicines, even at the highest dilutions, differ from their controls; they can no longer be considered as pure solvents and different starting materials can be discriminated.[9–19] In addition, NMR suggested for the first time the presence of nanometric superstructures,[19] which was further confirmed by evidence of the involvement of nanobubbles.[14,17] Then, Chikramane et al[20] showed by transmission electron microscopy (TEM) the presence of nanoparticles (NPs) in commercial ultra-high dilutions of 30cH and 200cH metal-based homeopathic medicines.

Nanostructures and/or NPs are now widely confirmed,[21–32] and we know that these structures are charged and polarised[27,33,34] and that long-lived sub-micrometric bubbles have been demonstrated in shaken and very highly dilute solutions.[29] However, there is considerable disparity and even discordance in studies on the nature and size of these NPs, as previously discussed.[35] These discrepancies are due to the different techniques used (atomic force microscopy, TEM, EM scanning, NP tracking analysis [NTA], dynamic light scattering [DLS], selected area electron diffraction, energy dispersive X-ray [EDX] microanalysis) and/or to the preparation method, especially when the samples come from unspecified commercial production or are prepared in ethanol medium.[24,32] In general, NPs ranging from 1 to 2 nm to tens and even hundreds of nanometres have been shown: for example, there has been a lack of coherence for the same 6cH dilution in different papers: 1–15 nm, 90 nm or 150–300 nm. Technique-related artefacts were identified. In addition, the alleged nature of these NPs was highly inconsistent, comprising either essentially water structures, particles containing silica or, paradoxically, particles containing measurable amounts of the original substrate in ultramolecular dilutions up to 200cH.[19,20,24,27,31,32]

With the aim of clarifying the situation, we launched the DYNHOM project in 2014. Through a multidisciplinary approach, in collaboration with universities, our main goal has been to describe and characterise homeopathic medicines up to their highest dynamisations. Various approaches have been combined: structural (NMR), particulate (NTA), material (scanning electron microscopy-EDX) and molecular (Fourier transform infrared spectroscopy [FTIR])—all this without excluding the study of electric fields and other approaches to the nature of homeopathic medicine. In this publication, we focus on the study of particles.

In 2016, we tested DLS[36] with the aim of visualising very small NPs in potencies of *Cuprum* and *Gelsemium*.[23] The sizes of NPs in *Cuprum* 4cH were of the same order as those in Lactose 4cH and a simple dilution (10^{-8}) (between 0.8 nm and 1.9 nm) and could not be distinguished. Above 4cH, the results in this size range were no longer significant as they were within the margin of error of this technique. On the other hand, NPs of 100 nm and larger were observed by DLS over the whole dilution-dynamisation range (5–30cH and 200K). 100 nm is the best size range for the application of the NTA technique.

The aim of the present study was to verify all our NP measurements[23] carried out over the last 8 years on several homeopathic medicines and controls, using different approaches, and to try to gain an idea of their nature. All these dynamised medicines (DYNs) are produced according to Good Pharmaceutical Practice on six different production lines up to 30cH potency and compared with dynamised solvent controls and simply diluted (DIL) samples. This paper has focused on a specific technique (NTA), considering only new unpublished data we have collected since 2018.

The potentisation process is carried out using a validated machine that provides 100 calibrated vertical shocks at each dilution. Successive potencies are made in a new container at each step. The dilution process is carried out by adding 1 part of the material to 99 parts of the solvent (cH potency). An 'n' cH potency corresponds to a 10^{2n}-fold dilution, so the theoretical limit of the molecular presence of the starting material is obtained at 12cH.

Materials and Methods

Rationale: Anticipating the need to detect low concentrations of poly-disperse particles of different sizes and shapes, we used NTA. For these measurements, we used the NanoSight NS 300 Malvern instrument and software from Sysmex installed in our measurement laboratory in Chastre (Belgium). This instrument can be used to measure NPs between 20 and 1,000 nanometres in aqueous solutions (maximum permitted ethanol content of 10% v/v). For this reason, we worked exclusively with pure water as diluent medium. This new technology has been validated,[36] and several publications confirm its value.[26,37–40]

Aqueous potentisations or simple aqueous dilutions are drawn into a sterile 1 mL syringe. This is placed in a syringe pump, which ensures that the solution passes at a constant speed through a small cell crossed by a beam of laser light at a wavelength of 488 nm. The Brownian motion of the particles is observed by a camera during five random sequences of 1 minute each. This observation can be followed and recorded on the computer screen. One minute of observation corresponds to 1,500 measurements of the visual field (frame). For each field, the number of particles, their size,

the intensity of the light they scattered and the concentration of particles per millilitre are recorded.

The software locates numerous individual particles and calculates their hydrodynamic diameter using the Stokes–Einstein equation. The NanoSight instruments provide high resolution measurements of particle size, concentration, aggregation and scattered light brightness. These features enable real-time monitoring of minute variations in the characteristics of particle populations, while providing visual validation of these analyses. The results are the standard distribution, LD90, LD10 and LD50, which correspond, respectively, to the 90th percentile, 10th percentile and median of the particle sizes, with their respective margins of error.

The number and size of particles can be used to calculate their particle size distribution (Span). Span is a validated parameter of particle size distribution.[39] The Span formula gives an indication of the distance between the 10th and 90th percentile, normalised to the centre:

$$\text{Span} = (\text{LD90} - \text{LD10})/\text{LD50}$$

The first step was to compare the NTA measurements of different controls. The solvent is initially aqueous if the raw material is soluble in water (*Kalium muriaticum*) or hydro-alcoholic (*Gelsemium*, *Pyrogenium*) or is lactose for a preliminary trituration phase for insoluble materials (*Cuprum*, *Argentum*, *Silicea*). The container could be glass or PET (polyethylene terephthalate). Data from different source materials were considered.

Homeopathically Manufactured Medicines

The medicines and controls were produced in our own laboratory in Wépion (Belgium) using a validated (ISO 5) laminar flow (Thermo Heragard Eco 1.2 horizontal B75/180). Our pharmacist followed the European Pharmacopoeia, which describes exactly how the manufacturing process must be carried out according to the homeopathic tradition. The pharmacist's equipment included a mask (possible toxic effects on the respiratory tract), protective goggles (possible irritating effects of emanations during the crushing process, for example), shoe protectors, a white apron, no perfume, a hat and gloves. Hands were washed thoroughly before each operation.

(a) For soluble starting materials, including ethanolic mother tinctures (ethanol, *Gelsemium*, *Pyrogenium*, *Kalium mur*), all dilutions (dynamised or simply diluted) were made in pure water, except for the first one made with the same alcoholic strength of the stock. The water used was deionised water taken directly from the tap, after first releasing some water. The tip of the tap spigot went directly into a flask containing ethanol to avoid ambient contamination. To rinse the tip, we let the water run into the sink before taking a sample. The purification apparatus was a Merck Elix70, reference ZLXS50070, F6KA83559A, 230 V, 50 Hz. The brown 30 mL pharmaceutical flasks used were made of soda–lime–silicate glass (ISO-719, ISO4802-1, Ph-Eur 3.2.1.; USP <660>: ≤0.85 mL 0.02N HCL/g), sealed with tight plastic drop caps with a screw-on polypropylene closure system (Aceso® PPM H250 grade). All steps were performed in new 30 mL glass vials after washing and passage through a high temperature dryer. The brown PET bottles (60 mL) used for special controls were manufactured according to ISO-9001 standards and closed with a polypropylene closure system (PhEur 3.1.3 'Polyolefins'; PN*18*K*S1 0.6 of PPH). The dynamisation process was performed (100 ± 1 shocks in 2 seconds) using a Labotics© certified and validated dynamiser 'Dynamat©'. Gilson branded micropipettes were PipetmanP Gilson P200, 50 to 200 µL; and PipetmanP Gilson P1000, 200 to 1,000 µL, with suitable disposable tips. The simple dilutions used as complementary controls were prepared in the same way, but without the dynamisation process. By simply turning the vial upside down once, a simple and gentle manual mixing process was achieved.

(b) For the insoluble starting materials (*Cuprum*, *Argentum*, *Silicea*), the first two or three triturations were performed manually according to the standardised rules and controls of Good Pharmaceutical Practice. We used monohydrated, moderately fine lactose (medium particles of 240 µm) from ABC Chemicals (Aut.84GIR05797; Ph. Eur. Lot 19I04-B02-194990; Exp. 30-04-2022; Cond. 30-10-2019). Subsequent dilutions were made with water as described above. The potentised lactose samples used as controls were prepared in the same way, including the first three triturations by mixing 100 mg of raw material with 9.9 g of pure lactose to produce the 1cH. The simply diluted controls were prepared by the same sequential steps after three triturations. Further dilutions were prepared in water, but without the dynamisation process.

(c) Each vial was labelled with an abbreviated code for the raw material, including the level of dilution or potentisation, line number and date of manufacture.

(d) Six production lines were prepared on the same day with a single batch of water.

A summary of the manufacturing procedures for the dynamised lactose, water and alcohol controls is given in ►**Table 1**.

Randomisation and Blinding

As the measurements were performed on a total of 2,532 samples (six production lines for each drug and/or controls), repeated five times – that is, 12,660 NTA measurements – the risk of error in a double-blind approach became very high in practice. The first NTA measurements started in the year 2018; complete measurements for a single production line took at least 6 weeks. For this reason, we preferred a more reliable approach where each bottle was labelled with the short code given by the pharmacist before the samples were taken to the laboratory for NTA measurements. The full label was applied when the results were entered into the Excel file.

Table 1 Residual concentrations of lactose or alcohol in all samples

Stock	Solid potentisations	First liquid potentisation	Next potentisations	Maximal initial content in 9cH
Aqua		1cH aqueous 200 mg in 19.8 mL	2 to 30cH aqueous 200 µL in 19.8 mL	0
Monohydrate lactose	Triturations 1 to 3cH 100 mg in 9.9 g 1 h trituration	4cH aqueous 200 mg in 19.8 mL	5 to 30cH aqueous 200 µL in 19.8 mL	2.775×10^{-12} M
Ethanol max 70% V/V		1cH aqueous (ethanol max 70%) 200 mg in 19.8 mL	2 to 30cH aqueous 200 µL in 19.8 mL	max 1.35×10^{-16} M

Note: As solvent is always pure water, after some steps more, lactose and alcohol disappear completely during the manufacturing process.

Nanoparticle Tracking Analysis

The mathematical analysis of the results of high-resolution measurements of particle size, concentration, aggregation and scattered light brightness was carried out by the first author under the supervision of the team and external experts. The number and size of the particles and their size distribution (Span) were calculated.

Above all these parameters, an asymmetry coefficient (AC; LD50/mean size) is calculated to compare the evolution of the size distributions in the different production lines. A decrease in the AC indicates an asymmetry in favour of larger NPs and *vice versa*.

The brightness intensity of the particles is an indication of their nature. For example, a large nanobubble refracts light more intensely than a smaller nanobubble, but a particle of matter will have its own luminosity, *a priori* less than air bubbles. This parameter has only been validated for homogeneous particle solutions. For a mixture of particles, discrimination will be much more difficult because of the dual dependence on both nature and size: only large differences in intensity should be considered.

Mathematical Calculations and Statistical Analysis of Results

Since we wanted to show the evolution of particles in a step-by-step manufacturing process, we used a data transformation that transforms an apparently noisy set of points into a smooth curve (►**Supplementary Fig. S1**, available online only).[12,41,42] In a step-by-step production line, each value depends only on the number of particles or particle distribution (Span) that precedes it. This data conversion is derived from a cumulative arithmetic mean and is hereafter referred to as the Contonian Lagrangian frequency (*H*). The conversion calculations take into account each of the individual measurements made for each dilution/dynamisation on each production line. '*H*' is more than the sum of the averages. For each production line, each value is compared to its predecessor to calculate its *H* value, and then, these *H* values can be aggregated. *H* is calculated thus[42]:

$\int_{V_0}^{V} x(u)du = L(V)$ with $x(u)$ being the observed character and u the dynamisation or dilution. This integral will be the Contonian Lagrangian. The aspect of the curves $L(V)$ will be linear, and we can calculate the Contonian frequency parameter *H*, since the Conton is defined by the equation:

$\exp\left(iH\int_{V_0}^{V} x(u)du\right)$ and represents the point of the circle that varies as a function of the Hahnemannian parameter (the dilution level) in a circular movement:

$\theta = H\int_{V_0}^{V} x(u)du$ where Θ is the polar angle of a point of value equal to the *v* parameter. The second step of the practical construction of a Conton consists of the adjustment of the *H* frequency to get, in the complex plane, a continuous trajectory. The *H* value so determined is called the Contonian frequency.

$H = 2^{*}\pi/L(Xn)$ summarises this approach to the Contonian frequency.

The lack of singularity (discontinuity, large fluctuations) and the very different Lagrangian frequencies (*H*) for the solvent and for the molecule diluted in the same solvent can only lead to the conclusion that the observed phenomenon not only exists but is specific to each diluted product and not related to the classical chemical behaviour of the compound.

SigmaStat version 4, which allows multiple statistical procedures, was used for conventional statistical analysis. In a first step, a three-way analysis of variance (ANOVA) and Tukey's tests were applied to the raw data, even if these tests are not strictly applicable due to the non-Normality of the data. A significant effect is detected only for the factor 'product' (►**Supplementary Tables S1–S4**, available online only). After the transformation of the data, the *H*-values calculated from the dilution series for the six manufacturing lines and the different products were analysed using a two-factor ANOVA after checking that the tests for Normality (Shapiro–Wild) and equality of variances (Brown–Forsythe) were passed. If the test was significant, a pairwise comparison was made (Holm–Sidak method). The significance level was set at 0.05.

Results

Nanoparticle Tracking Analysis in Controls

The presence of NPs is a common denominator when a dynamisation process is used in the manufacture of homeopathic dilutions. This was also observed in the

potentised controls of our current study. Using two types of containers, we found that the number, mean size and size distribution (Span) of these particles were strongly dependent on the nature of the controls and the containers used (►**Fig. 1**).

Nanoparticle Tracking Analysis in Homeopathic Dilutions

NTA revealed the presence of particles in all diluted or potentised samples, whereas an unreliable number of particles was detected outside the margin of error in the pure

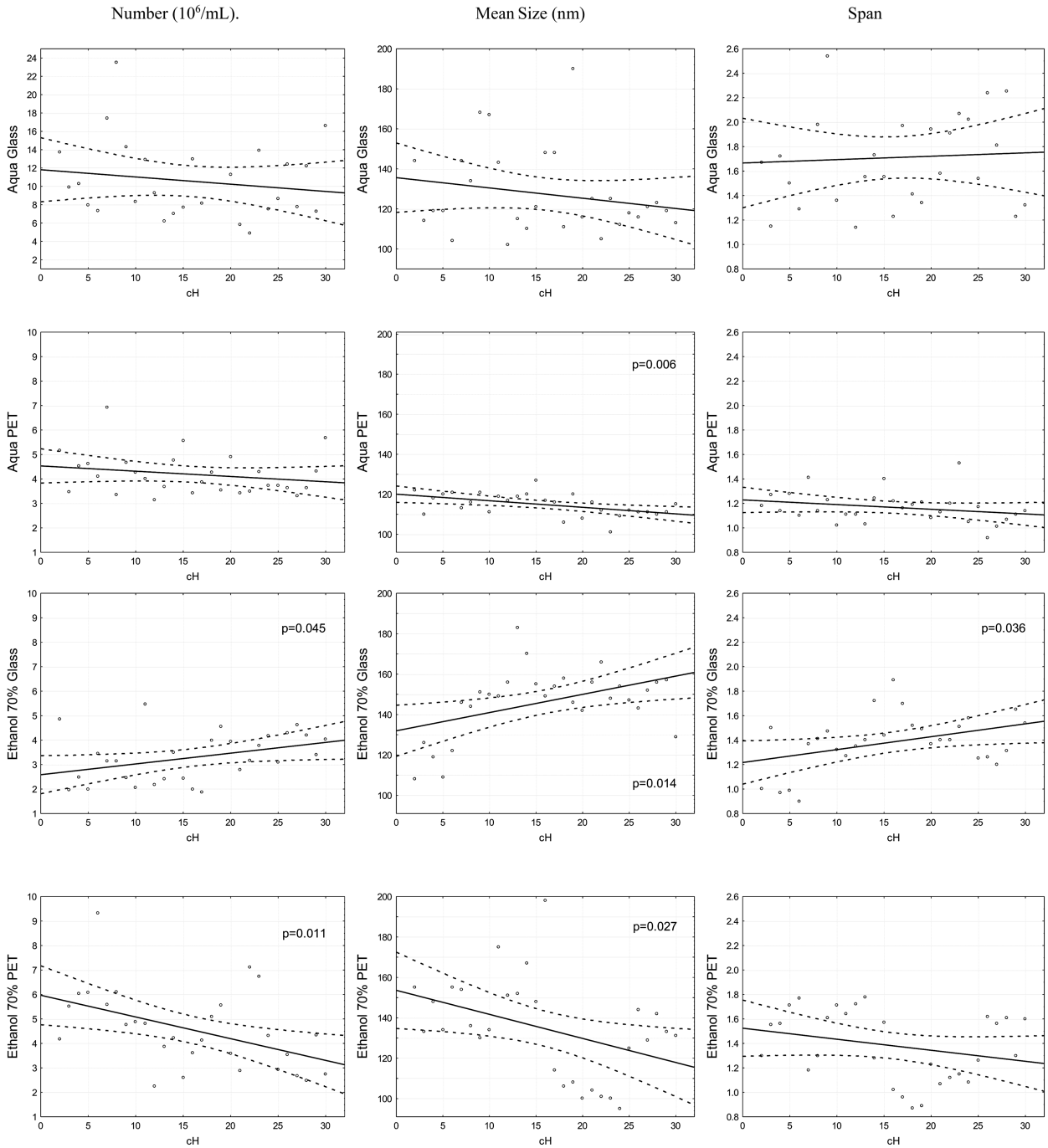

Fig. 1 Mean number (N), size (S) and size distribution (Span) of particles for six pooled manufacturing lines of *Aqua pura* and ethanol controls in glass and in PET containers.
Mean values of the six lines are plotted and fitted by a linear regression function with 95% confidence limits. Pure dynamised water in glass bottles allows the formation of very large quantities of NPs, around 12 million per mL. In PET bottles and when mixed with initial alcohol, as well as in glass bottles, we obtained three times fewer particles. For pure water in glass, the number and size distribution of particles were large but stable through the potentisation process. The sizes of NPs showed a tendency to decrease in glass, but decreased significantly in PET. Ethanol–PET and ethanol–glass showed completely opposite behaviour: increase in number, size and Span with potentisation in glass, but decrease with potentisation in PET. Ethanol in glass was the only case where N, S and Span increased with potentisation. Note that the dilution medium was pure water in all cases.

water control directly from the tap (0.2 ± 0.1 particles/frame). In the following, we will examine how potentised samples differ from diluted samples and controls, and how dilutions of directly soluble raw materials differ from those of insoluble raw materials, which require a previous trituration step for their preparation.

Size of Particles

Particle sizes evolved differently as a function of dilution, depending on whether trituration was required (*Cuprum*, *Argentum*, *Silicea*) or not (*Gelsemium*, *Pyrogenium*, *Kalium mur*) (►**Fig. 2**). Except for *Gelsemium*, which showed a discrete downward trend ($p = 0.051$), all dynamised samples showed a significant increase in size with dilution (range $p = 0.015$ to 0.001; *Pyrogenium*, not shown in the figure, $r = 0.507$; $p = 0.006$), in contrast to directly soluble samples, showed a decrease or non-significant variations in half of the cases. In addition, the mean particle size was significantly smaller than controls for soluble ingredients (mean size 146.1 and 127.6 nm, for ethanol and water controls, respectively) and larger for insoluble ingredients (mean size 104.8 nm for lactose). These differences persisted significantly beyond 11cH (►**Table 2**).

Size Distribution of Particles

The size distribution of the particles (Span) appeared to be characteristic of the stock and/or the manufacturing method (►**Fig. 3**). A dynamised production line could be distinguished from its controls (the dynamised solvent) or from the same simply diluted stock. The standard deviations of the Contonian frequencies (H) are remarkably small for the dynamised production lines and larger for the simple dilutions (►**Supplementary Tables S5** and **S6**, available online only). For insoluble solids (*Cuprum*, *Silicea*, *Argentum*), the Spans of the dynamised dilutions were systematically higher than those of the solvent, whereas the opposite was true for soluble solutes (*Kalium mur*, *Gelsemium*). The Spans of simply diluted solutions were above those of the solvent for triturated preparations and equal to or below those for soluble starting materials. The asymmetry coefficient AC (LD50/mean size ratio) of the size distribution provided additional information on the different behaviour of dilutions of soluble and insoluble raw materials (►**Table 2**). The observed differences in AC indicated the presence of different sub-populations of NPs generated by the dynamisation process. Strikingly, this was observed in high homeopathic potencies, where the initial material is no longer expected.

Number of Particles

An example of the effect of dynamisation on the number of particles is shown in ►**Fig. 4**.

The number of particles in the different lines of dilutions and controls is shown in ►**Fig. 5**. For simple dilutions, this number is approximately 2.5 million particles per ml. For dynamised dilutions, the number is close to 9 million per ml.

For soluble stocks, the number of particles was systematically higher in the dynamised production lines than in the controls. For insoluble materials, this number was lower than for the dynamised control and generally higher than for simple dilutions. Again, there was a difference in behaviour between soluble and insoluble raw materials. The differences were even more pronounced above 12cH, confirming the result in ►**Fig. 1** that the initial number of particles is a determining factor for subsequent dilutions.

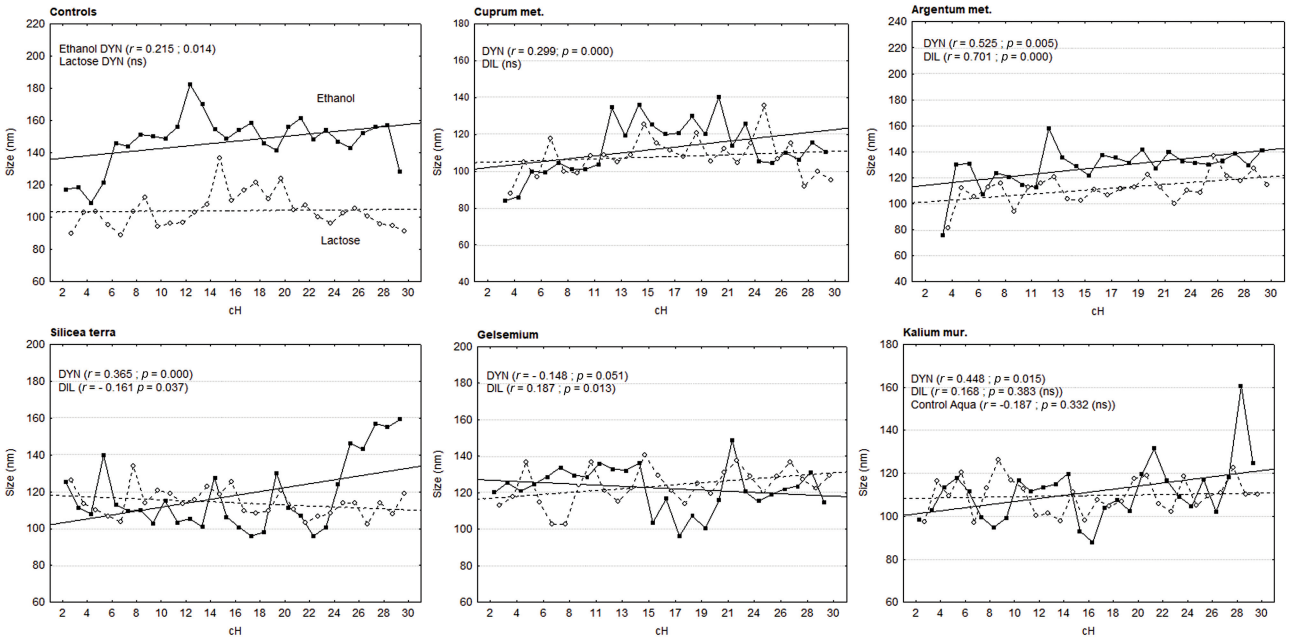

Fig. 2 Influence of the manufacturing process on the size of particles. Dynamisation (DYN): full line. Simple dilution (DIL): dashed line. Mean size values for six pooled lines of different raw materials are plotted as a function of the dilution amount and fitted with a linear regression function.

Table 2 Size of particles versus controls and asymmetry of the size distribution in ultramolecular dynamised lines and simple dilutions

	Size nm (cH > 11)			LD50/Mean (cH > 11)		
	Stock	Control		DYN	DIL	
Cuprum	120.1 ± 14.1	107.0 ± 13.7	↗ $p < 0.00001$	0.864 ± 0.032	0.850 ± 0.084	↗ $p > 0.05$
Argentum	134.6 ± 12.9	107.0 ± 13.7	↗ $p < 0.00001$	0.866 ± 0.025	0.853 ± 0.045	↗ $p > 0.05$
Silicea	121.1 ± 32.3	107.0 ± 13.7	↗ $p = 0.0003$	0.873 ± 0.025	0.869 ± 0.072	↗ $p > 0.05$
Gelsemium	118.9 ± 19.1	153.4 ± 23.1	↘ $p < 0.00001$	0.868 ± 0.042	0.877 ± 0.025	↘ $p > 0.05$
Pyrogenium	147.9 ± 19.1	153.4 ± 23.1	↘ $p > 0.05$	0.821 ± 0.050	0.866 ± 0.035	↘ $p = 0.005$
Kalium mur	113.7 ± 25.3	123.1 ± 40.6	↘ $p < 0.038$	0.859 ± 0.105	0.867 ± 0.050	↘ $p > 0.05$

Abbreviations: DIL, dilution; DYN, dynamisation.
Note: For each raw material, six production lines were measured. Grey lines indicate insoluble ingredients. Differential features were clearly found. Arrows indicate the qualitative direction of variation, comparing dilutions versus controls and dynamisation versus simple dilution. Statistical discrimination was performed using a pairwise *t*-test and a Kolmogorov–Smirnov test to assess Normality. *Size nm (cH>11)*: Larger sizes than controls for insoluble raw materials and smaller sizes for soluble raw materials. *LD50/Mean (cH>11)*: Using the asymmetry coefficient AC = LD50/mean size, two different patterns of NP populations were observed, showing that the dynamisation process had an opposite effect on these two types of starting materials. A higher AC favours a sub-population of smaller NPs in the dynamised lines compared to the simply diluted lines, and vice versa.

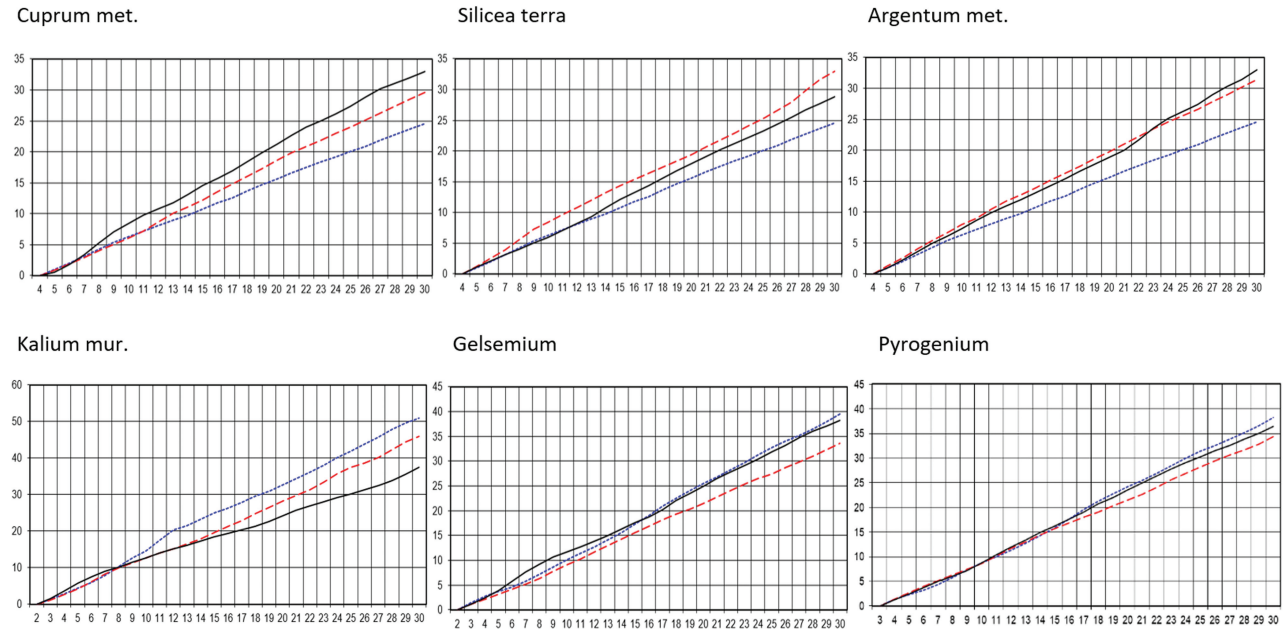

Fig. 3 Particle size distribution (Span) as a function of the manufacturing process for different raw materials with comparison to the dynamised controls. (cH dynamisation ---, simply diluted —, dynamised solvent ···). Each line in the graphs represents six pooled manufacturing lines, up to 30cH for each raw material or solvent; for simply diluted lines the degree of dilution is comparable. On the x-axis are the dilution/dynamisation levels and on the y-axis are the cumulative Lagrangian (*H*) values obtained at each stage of the manufacturing process.

When differentiation was not possible with a single parameter, integration of other NTA parameters extended the statistical discrimination between different starting materials and controls and became even more apparent, especially at very high dilutions (►**Table 3**).

Morphological Features of Particles

►**Fig. 6** shows some examples of images observed with NTA. Particles were either isolated or grouped by two or three others, or in longer and more static chains. These morphological features were exhaustively counted from the films of the 9cH and 24cH dynamised samples and the 10^{-18} and 10^{-48} simply diluted samples to compare low and high dilutions (►**Table 4**).

Scattering Light Intensity of Particles

During visualisation, the particles showed varying degrees of brightness. In the NTA technique, the scattered light intensity (SLI) of the particles is expressed in arbitrary units (a.u.), as specified by the manufacturer. Looking at the distribution of the scattered light intensities of the particles in our samples, we could roughly observe several different groups. Some showed a

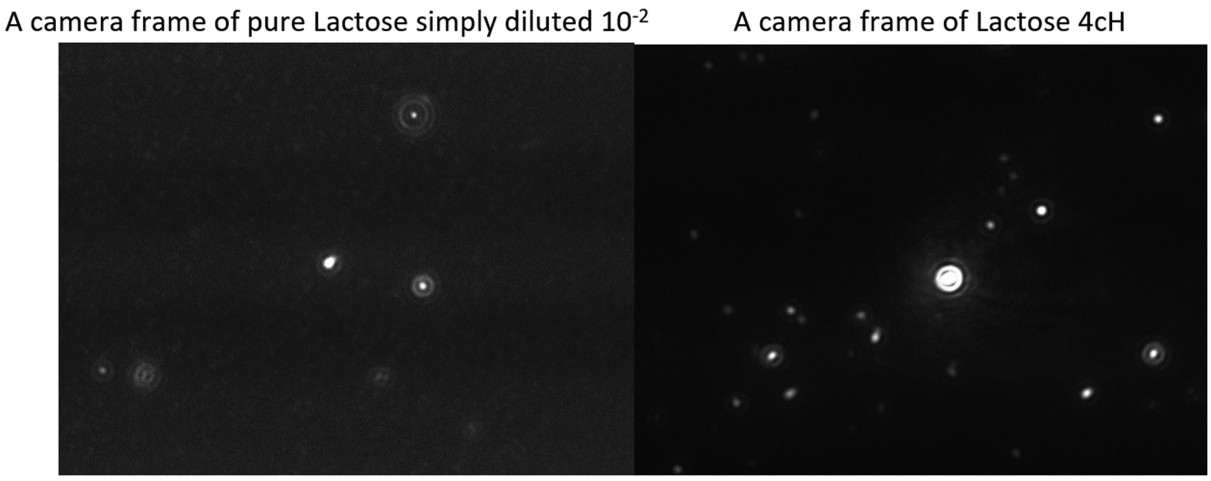

Fig. 4 Examples of particles passing in front of the NTA laser camera for an identical concentration of lactose. The 4cH lactose sample was obtained by dilution/dynamisation in water from a third trituration of lactose. The crude amount of lactose was therefore the same as in a simple centesimal dilution of pure lactose. There were significantly more particles in the dynamised preparation and the particle size distribution was wider.

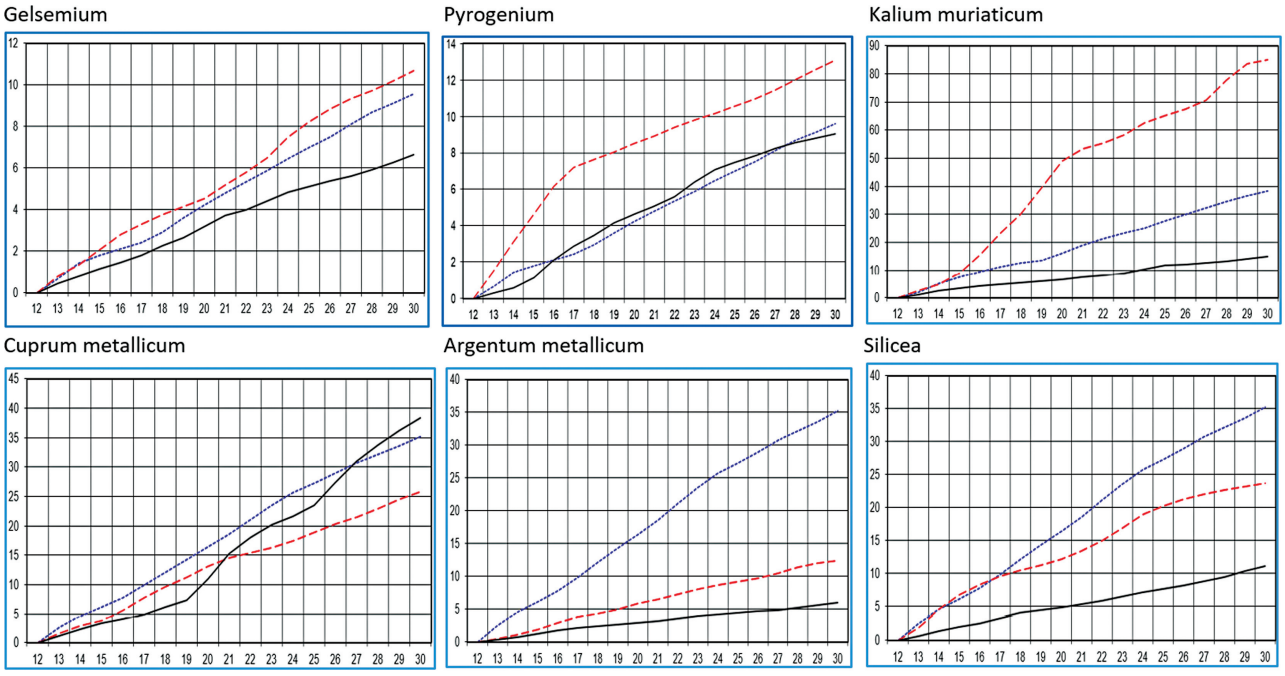

Fig. 5 Example of Lagrangian representations of number of particles in ultramolecular dilutions for different manufacturing lines (cH dynamisation —, simply diluted —, dynamised control ...). Each line of the graphs represents six pooled production lines. On the x-axis are the dilution/dynamisation levels and on the y-axis are the cumulative Lagrangian (*H*) values obtained at each stage of the manufacturing process. The linearity of the results is less obvious for particle numbers than for particle sizes, indicating greater measurement variability. For soluble materials, the number of particles was systematically higher in the dynamised production lines than in the controls. For insoluble materials, this number was lower than for the dynamised control and generally higher than for simple dilutions.

good distribution of NP scattering intensities, while others formed clusters of NPs with low intensity and small size (►**Fig. 7**).

This finding suggests that the nature of the particles may differ from one production line to another and from one raw material to another. However, the isolated SLI parameter alone did not allow a clear distinction to be made between a dynamised production line and a simply diluted one, or between high and low dilutions. But the analysis of the distribution of scattering intensities, in particular through an asymmetry index (LD50/max SLI ratio), allowed us to detect specific features of particle populations in dynamised samples and in high dilutions (►**Table 5**). Except for *Kalium mur*, dynamisation induced a sub-population of NPs with higher SLI compared to simple dilutions, and the highest dilutions (24cH) appeared less intense than the lowest (9cH).

Table 3 Discriminant statistical analysis of Span and number of particles between raw materials and controls for all, and high dynamisations (above 11cH).

		Span				Number of particles			
		All		>11cH		All		>11cH	
	Comparison	*q*	*p*	*q*	*p*	*q*	*p*	*q*	*p*
Lactose	*Argentum met* cH *vs.* Lactose cH	7.36	<0.001	6.26	<0.001	13.47	<0.001	17.41	<0.001
	Argentum met cH *vs.* Argentum met DIL	1.01	>0.05	2.11	>0.05	11.56	<0.001	28.42	<0.001
	Cuprum met cH *vs.* Lactose cH	5.30	<0.001	4.98	0.001	3.45	0.019	4.67	0.002
	Cuprum met cH *vs.* Cuprum met DIL	3.69	0.004	3.59	0.005	1.84	>0.05	5.44	<0.001
	Silicea terra cH *vs.* Lactose cH	7.58	<0.001	8.90	<0.001	6.25	<0.001	3.17	0.010
	Silicea terra cH *vs.* Silicea terra DIL	3.33	0.008	2.27	0.047	14.74	<0.001	11.10	<0.001
Ethanol	*Gelsemium* cH vs. Ethanol cH	3.77	0.011	4.1	0.006	3.36	0.021	0.97	>0.05
	Gelsemium cH *vs.* Gelsemium DIL	2.67	0.047	2.09	>0.05	2.55	>0.05	4.65	0.003
	Pyrogenium cH *vs.* Ethanol cH	4.25	0.005	6.08	<0.001	6.89	<0.001	3.17	0.020
	Pyrogenium cH *vs* Pyrogenium DIL	2.43	>0.05	2.91	0.016	8.65	<0.001	3.72	0.012
Aqua	*Kali mur* cH *vs.* Aqua pura cH	0.59	>0.05	0.09	>0.05	2.62	0.026	2.09	>0.05
	Kali mur cH *vs.* Kali mur DIL	2.70	0,044	3.42	0.013	5.79	<0.001	8.37	<0.001

Abbreviation: DIL, dilution; $p > 0.05$ means non-significant discrimination using calculated '*H*' values.
Note: By integrating some NTA results (Span and number of particles) from several production lines, it was possible to significantly discriminate between dynamised samples, their controls and simply diluted samples, even in HDs, using 2-way ANOVA followed by pairwise comparison (Holm-Sidak method).

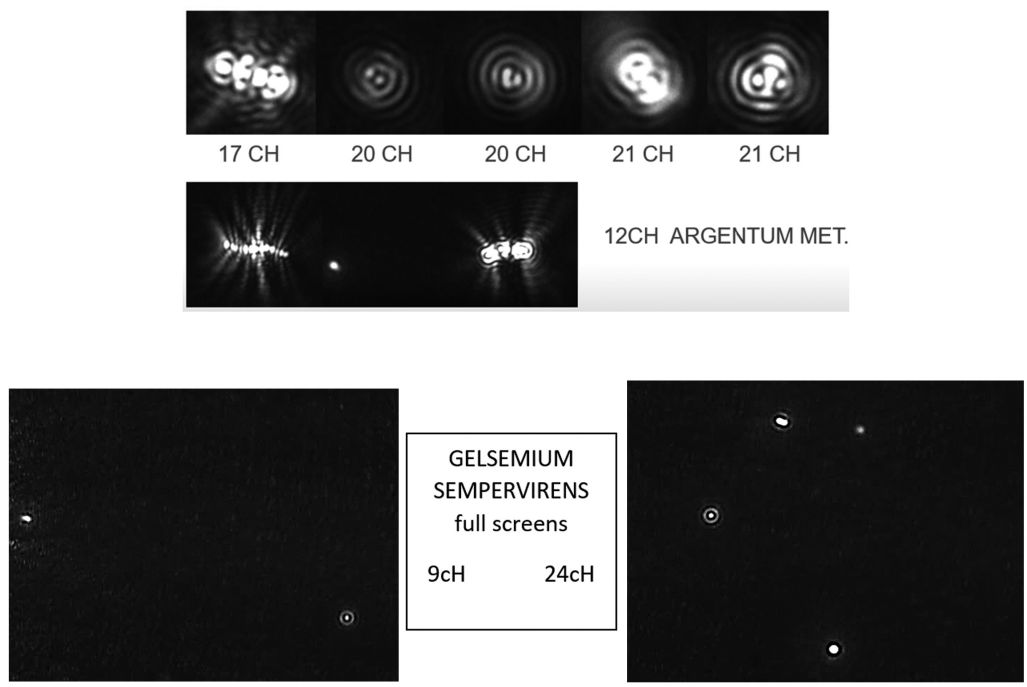

Fig. 6 A few examples of images observed with NTA. In these examples taken from the dynamised *Argentum* stock NTA films, the visualised particles were either isolated or grouped in two or three rotating around each other, or in longer and more static chains. Other isolated particles, faster in the flow, were not attracted by these clusters at all. Looking at one of the 1,500 frames obtained from the same production line of *Gelsemium*, in low and high potentisations, we observed a greater variety of shapes in the high dynamisations. Looking at all 1,500 frames in all their aspects we could define several particle features.

Thus, dynamisation and dilution led to different sub-populations of NPs, but here without different behaviour between soluble and insoluble raw materials. Unexpectedly, the particle size had little influence on the intensity of the scattered light.

Summary of Particle Measurements with Nanoparticle Tracking Analysis

All the particle measurements summarised in ►**Table 6** allowed us to observe clear differences in particle characteristics (number, size, size distribution, intensity of scattered

Table 4 Detection of aggregates or particle chains in dynamised and simply diluted samples of the different raw materials with comparison between high dilution (HD) and low dilution (LD) levels

	Cuprum	*Argentum*	*Silicea*	*Gelsemium*	*Pyrogenium*	*Kali mur*
Chains HD/LD (24cH/9cH)	0 / =	+ / ↗	0 / ↗	+ / =	+ / ↗	0 / ↗
Aggregates HD/LD (24cH/9cH)	+ / ↗	+++ / ↗	+ / ↗	++ / ↗	+++ /↗	+ / ↘
Chains DYN/DIL (9cH + 24cH/10^{-18} + 10^{-48})	0 / =	+ / ↗	0 / ↗	0 / ↗↗	++ / ↗↗↗	0 / ↗
Aggregates DYN/DIL (9cH + 24cH/10^{-18} + 10^{-48})	++ / ↗↗	++ / ↗↗	++ / ↗	+ / ↗↗↗	++ / ↗↗	++ / =

Abbreviations: DIL, dilution; DYN, dynamisation; HD, high dilution; LD, low dilution.
Note: For the counting, we observed 5 minutes of film per sample, six production lines: that is, 30 minutes of film for each dynamisation or simple dilution. The left symbol (+) indicates the number of a type of feature counted and the arrows the direction of its variation when comparing HD vs. LD or DYN vs. DIL. The number of aggregates and chains increased in HDs and dynamised samples in almost all cases.

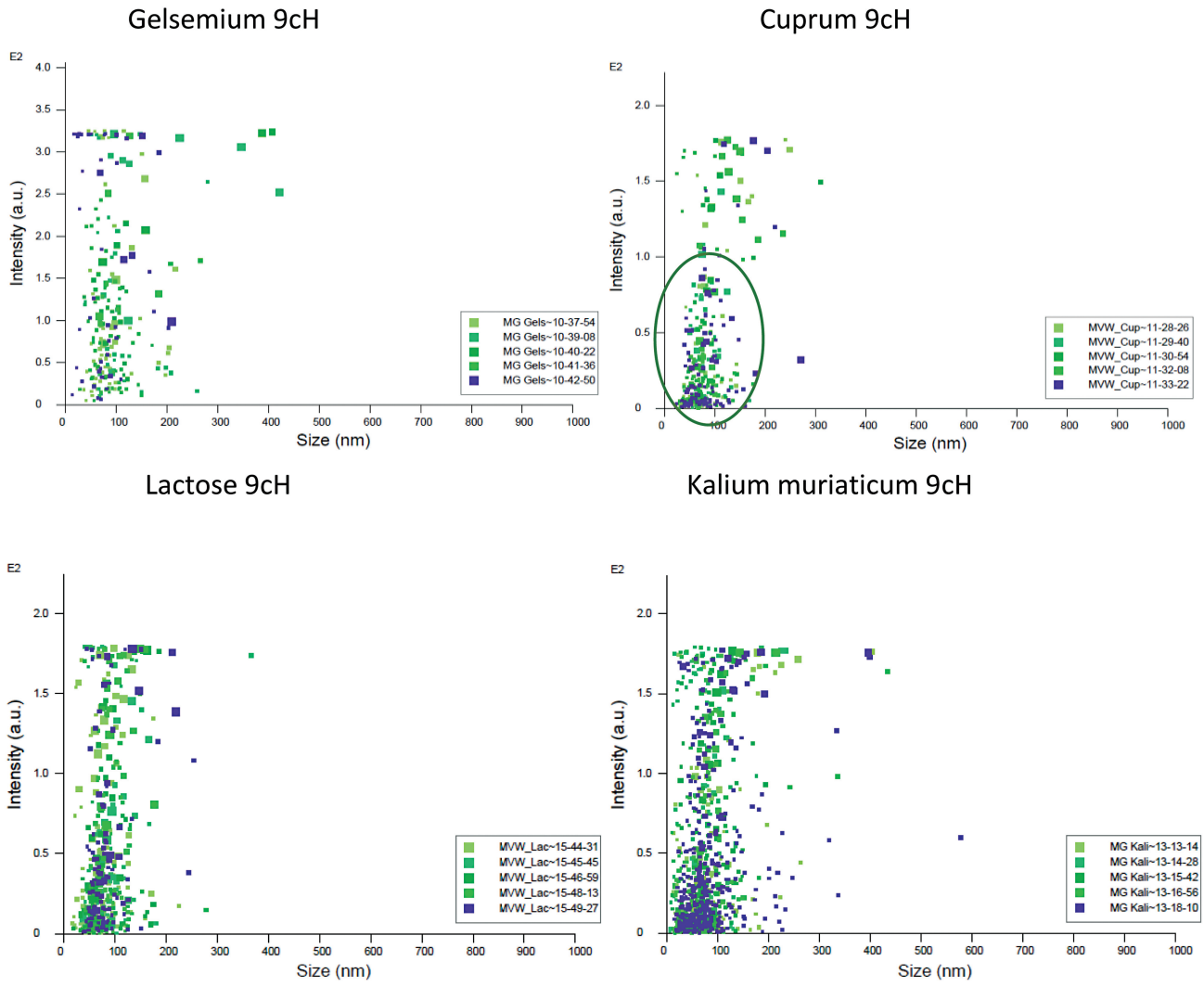

Fig. 7 Examples of five successive scattering light intensity measurements in arbitrary units (a.u.) (production line 'a'). Brightness intensity expressed in a.u., factory setting by manufacturer, versus particle size in nm. Overlay of 5 minutes of observation (1 measurement = 1 minute = 1,500 frames). *Gelsemium* 9cH shows a wide range of particle sizes, with particles appearing at all scattered light intensities. *Cuprum* 9cH shows a marked clustering of particles at low scattering light intensities and NPs sizes, especially at half the intensity scale of *Gelsemium*. Compared to all our measurements, lactose control 9cH showed the best intensity distribution and *Kalium muriaticum* 9cH the best example of clustering of small NP sizes and low scattering light intensities. In our samples, note that the particle size has little effect on the intensity of the scattered light. This suggests that the intensity of the emitted light depends more on the nature of the particles than on their size.

light, attraction of particles forming aggregates or chains) depending on the production process of soluble and insoluble raw materials. We were also able to distinguish between high and low dynamisation by combining several parameters. Although not all the directions of change shown in this table have been established by statistical tests, their consistency in distinguishing between insoluble and soluble materials can be considered as statistically valid.

Table 5 Maximum scattered light intensity (SLI) and median values in a.u. for six manufacturing lines of different raw materials and controls

		Max	LD50	LD50 / Max ratio (%)		
				%	Δ HD/LD	Δ CH/DIL
Lactose control	9cH	180	53	30		
Lactose control	24cH	180	44	25	↘	
Cuprum	9cH	180	46	25		=
Cuprum	24cH	180	51	28	=	↗↗
Cuprum	10^{-18}	180	40	22		
Cuprum	10^{-48}	180	24	13	↘↘	
Argentum	9cH	230	41	18		=
Argentum	24cH	330	51	15	=	↗
Argentum	10^{-18}	230	40	17		
Argentum	10^{-48}	330	34	10	↘	
Silicea	9cH	240	47	19		=
Silicea	24cH	240	35	15	↘	↗
Silicea	10^{-18}	240	49	20		
Silicea	10^{-48}	240	27	11	↘↘	
Ethanol control	9cH	330	64	19		
Ethanol control	24cH	330	61	18	=	
Gelsemium	9cH	330	69	21		↗↗
Gelsemium	24cH	330	58	18	=	↗
Gelsemium	10^{-18}	330	32	10		
Gelsemium	10^{-48}	330	41	12	=	
Pyrogenium	9cH	330	67	20		↗↗
Pyrogenium	24cH	330	52	16	↘	=
Pyrogenium	10^{-18}	330	45	14		
Pyrogenium	10^{-48}	330	50	15	=	
Aqua control	9cH	400	114	29		
Aqua control	24cH	240	48	20	↘↘	
Kali mur	9cH	180	30	17		=
Kali mur	24cH	330	33	10	↘	↘↘
Kali mur	10^{-18}	180	25	14		
Kali mur	10^{-48}	180	51	28	↗↗	

Abbreviations: DIL, dilution; HD, high dilution; LD, low dilution.
Note: The LD50, median intensity, is defined as the intensity above which there are as many particles as below, regardless of size. The ratio between this point and the maximum intensity allows us to compare the evolution of scattered light intensity between high and low dynamisation, and between dynamised series and simply diluted controls. A difference of >3% was arbitrarily used to assess a relevant variation. An increase in the ratio indicates the presence of a sub-population of higher brightness and vice versa.

Discussion

This study, which looked for NPs using the NTA technique, showed that homeopathic dilutions made using the dilution/dynamisation process are indisputably different from simple dilutions and from their diluted/dynamised solvent under the same conditions. This is the result of more than 12,660 measurements. We would like to point out that during these measurements all production factors were strictly controlled: same environment, same water source, same glass, same machines, same materials and same staff for each step of production and measurement—all of which reinforces the results. All dilutions were made using pure water. More than half of the dilutions were ultramolecular, beyond 12cH, in which we would expect no trace of the starting material.

Summary of the Main Results

Evidence of Nanoparticles

All samples tested and their controls, whether dynamised or simply diluted, showed NPs ranging from 20 nm (lower

Table 6 Summary of nanoparticle tracking analysis results

	Cuprum	*Argentum*	*Silicea*	*Gelsemium*	*Pyrogenium*	*Kali mur*
Size/Control						
All	↗	↗	↗	↘	=	↘
>11cH	↗	↗	↗	↘	↘	↘
Size (step by step cH)						
DYN	↗	↗	↗	*	↗	↗
DIL	*	↗	↘	↗	↗	*
AC DYN/DIL (>11cH)	↗	↗	↗	↘	↘	↘
Images (aggregates and long chains together)						
HD/LD	↗	↗	↗	↗	↗	=
DYN/DIL	↗	↗↗	↗	↗↗↗	↗↗↗	=
Span						
DYN/Control	↗	↗	↗	↘	=	↘
DIL/Control	↗	↗	↗	=	↘	↘
Number						
DYN/Control (>11cH)	↘	↘↘	↘	↗	↗↗	↗↗
DIL/Control (>11cH)	↘	↘↘	↘↘	↘	=	↘
DYN/DIL (>11cH)	↗ then ↘	↗	↗↗	↗	↗↗	↗↗
Intensity of scattering light						
DYN/DIL (9cH/10^{-18} | 24cH/10^{-48})	=|↗↗	=|↗	=|↗	↗↗|↗	↗↗|=	=|↘↘
HD / LD (24cH/9cH |(10^{-48}/ 10^{-18})	=|↘↘	=|↘	↘|↘↘	=|=	↘|=	↘|↗↗

Abbreviations: DIL, dilution; DYN, dynamisation. *non-significant (used when the difference is outside the error margin but does not reach an arbitrary cut-off of 10%.).

Note: All these particle measurements allow us to observe clear differences in particle characteristics (number, size, size distribution, intensity of scattered light, attraction or rejection of particles forming aggregates or not) depending on the manufacturing process of soluble and insoluble (grey background) raw materials. It is also possible to distinguish between high and low dynamisation by combining several parameters.

detection limit of NTA) to 300 nm (500 nm if we consider the extremes, average 100–140 nm). Only pure, unstirred water was free of NPs (►**Table 6**).

Influence of the Container

The type of container (studied only for water and ethanol solvents) has a considerable influence. For pure water, the number (N), size (S) and distribution (Span) of NPs in pure water are significantly lower in PET containers. For ethanol controls, the opposite behaviour was found with increasing dilution: increasing N, S and Span in glass and decreasing in PET.

Dilutions versus Controls

The samples, whether dynamised or simply diluted, differ from their controls (lactose, ethanol or aqua pura) in terms of N, S, Span and SLI. The differences persist and even increase beyond 11cH.

Dynamisation versus Simple Dilution

NPs differ in N, S, Span and SLI depending on whether the samples were dynamised or simply diluted. Numbers and sizes increased almost systematically with dilution for dynamised samples, but not for simply diluted samples. Dynamisation induced sub-populations of NPs with higher brightness. All differences persisted beyond 11cH. The occurrence of aggregates and chains of NPs was clearly enhanced by the dynamisation process and was found at the highest dilution levels.

Influence of the Nature of the Substrate

NPs differed significantly in terms of N, S and Span, with values even progressing in opposite directions during the dilution/dynamisation process depending on whether the substrate was directly soluble in water or in ethanolic solution (*Kalium* mur, *Gelsemium*, *Pyrogenium*) or required prior trituration in lactose (*Cuprum*, *Argentum*, *Silicea*). Sizes and Span were smaller than controls for soluble substrates and larger for insoluble substrates, whether samples were dynamised or not. A sub-population of NPs appeared to be larger for soluble substrates and smaller for insoluble ones. These results were demonstrated above 11cH.

About the Controls

The results of the controls shown in ►**Fig. 1** were very unexpected and therefore of the utmost importance. The only rational explanation for the findings is the involvement

of the atmosphere and elements from the glass in the formation of NPs. Several results seemed *a priori* unexplainable, such as the decrease of N, S and Span in PET containers as a function of dilution and the fact that the number of particles in the dilutions/dynamisations of the initial ethanol 70% in water and in glass always remained much lower than in the dilutions/dynamisations of water in glass, while the diluent in both cases was pure water. This suggests that the initial number of NPs determines the subsequent dilutions, even up to the ultramolecular range where the theoretical composition is pure water.

In view of these findings, any physical or biological study of homeopathic remedies must include as a control the corresponding solvent dynamised at all dilutions in the same type of container. This is what we have done in the present study, which may call into question studies using only non-dynamised water as a control. In particular, whilst the dynamised *Aqua pura* and lactose controls were relatively stable as a function of dilution level, ethanol diluted (or potentised) in water in a glass bottle (ethanol glass)—the control for dilutions of substances in ethanolic medium—showed a clear increase in the number and size of NPs. The influence of leaching glass elements and the atmosphere is undeniable. On the other hand, accepting that the PET wall cannot be involved, the NPs observed in Aqua glass, Aqua PET and probably also in ethanol PET are most likely composed of sub-micrometric or nanometric gas bubbles (nanobubbles, NBs). In ethanol glass, NPs of a different nature may be present, formed by complexes of the initial ethanol with NBs and elements released from the glass, as postulated by Demangeat[14,17] and discussed below.

In addition to the formation of air NBs, the atmosphere can also play a role by dissolving CO_2 and producing carbonic acid HCO_3—in any type of dilution, but with subsequent formation of bicarbonates and even insoluble carbonates if the container is glass, through interaction with the released elements. This has been demonstrated in our previous publications by EDX and FTIR,[43] which show significant amounts of carbonates in dilutions, but only insoluble carbonates are likely to produce NPs visible in NTA.

As for the findings in PET containers, the drastic decrease in N, S and Span of NBs could be due to the lowering of pH (as suggested by our not yet published pH measurements) and/or to the presence of HCO_3 anions, which modify the electrical properties of the air–water interface of NBs or even the surface tension.[44] However, the decrease in N, S and Span with further dilution remains unexplained. The discussion of factors influencing the number and size of bubbles is developed in the literature.[29,40]

The initial presence of ethanol in glass preparations was shown to drastically reduce the number of NPs. This is consistent with a study by Zhang et al[45] showing that nanobubbles decrease with ethanol concentration and disappear in $\geq$80% ethanol solution. For mixtures of water and organic chemical compounds such as ethanol, questions remain: are nanoentities, nanobubbles or NPs detached from surfaces; are they impurities; or are they a mix of both?[46–48]

About the Dynamisation Process

Whilst the dilution factor is part of the potentising process, it is the dynamisation itself, a manufacturing method specific to homeopathic medicines, that produces different NPs compared to simply diluted samples as controls. The first relevant result was that the number of NPs is higher in dynamised samples due to additional NBs induced by cavitation, which theoretically cannot occur in simply diluted samples (►**Fig. 5**). This could explain the higher brightness of NPs observed in dynamised samples (►**Table 5**). Furthermore, apart from *Gelsemium*, which showed a discrete downward trend ($p = 0.051$), the mean NP sizes increased significantly with the degree of potentisation, whereas simple dilutions showed a decrease or non-significant variations in half of the cases (►**Fig. 2**).

This result confirms Demangeat's NMR studies showing stable nanostructures increasing in size with potentisation in silica–lactose, histamine and lactose.[9,14,17] These nanostructures did not exist in pure dynamised solvents but only appeared in the presence of an initial solute, grew with potentisation and were destroyed by heating, supporting the involvement of NBs. Our own NMR work[12] and its review[9] confirmed changes in NMR relaxation times in favour of NPs of increasing size in lactose and *Gelsemium* dynamisations. The hypothesis put forward by Demangeat was that NBs were formed by cavitation during dynamisation, nucleating with the solute, with elements from the glass (essentially composed of SiO_2, Na_2O, Al_2O_3, Mg) and/or with other elements from the solution to form stable nanostructures or NPs. At each step of dilution/dynamisation, the pre-existing nanostructures or NPs act as nucleation centres for NB clustering and other elements from the medium, explaining the increase of NPs.

Another hypothesis emerges from the present study (►**Table 4**): NPs would increase in size by aggregation or even chain formation upon dynamisation, as it is known that NB-induced attractive forces are involved in the aggregation of particles.[49,50] Furthermore, NBs are known to coalesce,[51,52] and the entrapment of NPs by microbubbles and NBs has been directly demonstrated by high-speed videography.[30]

About the Nanoparticle Tracking Analysis Technique

NTA is a new and validated technique, which looks only at the 'particle' aspect of solutions. But we have used it methodically and repeatedly on a huge number of samples, giving our results a strength rarely matched in distinguishing between different types of dilution. NanoSight has been shown to be ideal for air NBs analysis and has even been claimed to be more reliable than DLS.[40] In a blinded experiment in which three samples of suspensions containing high, low and zero numbers of NBs were tested in duplicate, NanoSight results were found to be exactly as predicted.[39] The sizes of the NBs were around 100 nm[39] and 100–120 nm,[40] whereas no NBs were observed in distilled or tap water. Although the NTA technique is not intended to give any indication of the nature of the particles, we made unconventional use of the brightness data (SLI) provided by NanoSight and were able to

demonstrate no or very weak correlation between brightness and size, which favours the presence of NPs of different natures, corroborated in several cases by the existence of clusters of low-intensity particles (►**Fig. 7**).

About the Lagrangian Method and Contonian Frequency

The linearisation of experimental measurements according to the Lagrangian method described by R. Conte[42] was first used for the interpretation of the T1 and T2 relaxation times in NMR experiments.[12] This new mathematical procedure, which allows data to be plotted and statistical tests to be applied, was considered an important innovation by P Fisher in an editorial in 2017.[53]

Further studies using the classical statistical method multivariate ANOVA demonstrated the robustness of these earlier findings.[10] If we consider the assumptions for the application of the parametric test (ANOVA)—that is (1) Normality of the distribution, (2) equality of variances and (3) independence of the data—the third one cannot be met in the case of continuous series of homeopathic dilutions/dynamisations. The same applies to non-parametric tests such as Kruskal–Wallis one-way ANOVA. In fact, the measurements obtained by NTA for a given dilution are totally dependent on the previous values. In this context, the calculation of the Contonian frequency (*H*) obtained from the set of values of a series of dilutions/dynamisations is fully justified. This procedure is also very interesting for studying the consistency of different production lines of each product evaluated by means of the coefficient of variation (►**Supplementary Tables S5** and **S6**, available online only).

About the Nature of Nanoparticles

The results of the present study are strictly behavioural and do not allow any conclusions to be drawn about the nature of the particles observed. The PET data on dynamised water as a control—which *a priori* excludes any reactivity of PET with water—are only indicative of an interaction with the atmosphere: that is, generation of air bubbles and dissolution of air gases. Sub-microscopic and nanobubbles of air are therefore likely to be the main components of the NPs detected in this study.

However, the great variability in the physical properties N, S, Span, SLI of NPs, observed here – even above 11cH – and the ability to distinguish different initial substrates undoubtedly implies the presence of specifically induced NPs (►**Figs. 2**, **3** and **7**; ►**Tables 2** and **3**). Moreover, all the NMR studies mentioned above showed that nanostructures or NPs could not be isolated NBs, as they were never observed in identically dynamised controls; moreover, it should be remembered that ^{1}H-NMR relaxation is only sensitive to water and has identified ice-like water superstructures in homeopathic dilutions.[14,17] What is more, the NTA scattered light brightness analyses are in favour of particles of different natures (►**Fig. 7**, ►**Table 5**). If they were only air bubbles, we should have found a correlation between brightness and size.

We therefore conclude that the NPs observed here are a mixture of NBs (and/or sub-micron bubbles), complexes of NBs with molecules produced by the shaking, and NPs of material that may or may not be specific to the original substrate. Insoluble carbonates, derived from the dissolution of CO_2 from the air and demonstrated by Van Wassenhoven et al,[43] appear to be the most likely candidates for such non-specific NPs, present in all samples, whether dynamised or simply diluted. Furthermore, dynamised samples show the presence of a sub-population of NPs with different sizes, size distribution and scattering intensity compared to simple dilutions (►**Tables 2** and **5**). These sub-populations were significantly different, especially above 11cH, and consistently so, depending on whether the starting sample was triturated in lactose or pre-diluted in ethanolic solution. This observation remains unexplained. The clustering of NPs of lower brightness and smaller size, as shown in ►**Fig. 7**, may be in favour of composite NPs with a predominance of non-gaseous elements (silica, insoluble material). Conversely, large sizes and high intensities may correspond to isolated NBs or NB-rich NPs.

We have hypothesised here that some of the NPs may be isolated air NBs; however, we cannot state this with certainty. Due to their extremely high surface area/volume ratio, NBs exhibit peculiar adsorption properties with applications in many industrial fields, including water purification, froth flotation, surface cleaning, mineral and biomolecular separations.[54] Thus, most NBs can adsorb molecules from the medium, small NPs or impurities, which could explain the wide distribution of scattering intensities of NPs without any significant size dependence. In fact, the differentiation of NBs from other types of superstructures or NPs is not easy, and has been debated. Specific methods such as de-gassing, repeated filtration, compressibility and density measurements, freezing and thawing or long-term monitoring have been proposed to answer this question.[40,46–48,55,56] What can be said with certainty, however, is that our findings cannot be reduced to the mere formation of air bubbles. And even if they *were* nothing more than air bubbles, they stand out in a significant and specific way in the ultramolecular range, forcing us to admit that the potentisation process is not a mere dilution.

Limitations of Current Study

The present paper has focused on particles observable in NTA, but we already know that the dilutions contain many soluble molecules, mainly identified as sodium bicarbonate, which do not form visible particles.[43] Some particles may be generated by the NTA measurement system itself (contact with the syringe, thin tubing, slight turbulence), but these are common to all NTA measurements and cannot explain the different numbers and shapes of particles observed.

The six production lines, though separate, were not completely independent because the starting material came from the same single batch. A single set of controls (six lines each) was used for the different raw material production lines. The chains and aggregates observed in some lines could interfere with the interpretation of NP number, size and Span.

Though NTA can be used to differentiate between different manufacturing lines, it cannot be used alone to

distinguish one homeopathic raw material from another in a given dynamisation.

Implications for Future Research

The idea that homeopathic medicines are non-material, proposed both by opponents of homeopathy and traditional homeopathic practitioners, cannot be sustained in the light of these findings. Science is based on measurement; measurements are facts that cannot be disputed. But we should comment that the detection of NPs in high homeopathic potencies does not necessarily imply their biological activity (according to the idea of nanopharmacology or nanomedicine that has been raised[57,58]).

Another fundamental question remains to be understood: what is the nature of the information carried by these NPs, if any? What we are observing could be the carriers of specific information that we have yet to define. To further investigate the nature of these NPs, other physical methods, such as scanning electron microscopy and EDX-ray spectroscopy, NMR, infra-red measurements and electro-photonic analysis, are needed and are underway (see preliminary results[10,12,21,23,43]).

Conclusion

The NTA results confirmed that homeopathic medicines contain NPs with an average size of 100 to 140 nm in all dynamised or diluted samples, including dynamised solvents (except unstirred pure water). The number, size, size distribution and SLI of NPs proved that homeopathic potentisation is not merely a dilution. Dynamised liquid homeopathic medicines differ from simple dilutions and from their dynamised solvents, even more so in the highest potentisations above 11cH, with the additional presence of sub-populations of NPs of different size and brightness. NTA makes it possible to distinguish dilutions of insoluble raw materials, which require prior trituration, from substances directly soluble in ethanol or water, even in the ultramolecular 11-30cH range.

The nature of these NPs is not known, but they are most likely a mixture of sub-microscopic bubbles, complexes of NBs with elements from the glass and the atmosphere, and NPs of insoluble material including carbonates. Aggregates and chains of NPs are more abundant in high dilutions and dynamised dilutions. The nanoparticulate content of liquid homeopathic medicines appeared to depend on the raw material, the type of container used and the required production method. All the different NP characteristics were strikingly preserved at dilutions beyond Avogadro's number.

Highlights

- Particles in aqueous homeopathic medicines can be identified using nanoparticle tracking analysis measurements, even at ultra-high dilutions.
- Discriminant analysis between simple dilution and homeopathic potentisation is possible, proving that the homeopathic potentisation process is not plain dilution.
- Above Avogadro's limit, homeopathic solutions cannot be considered as pure water.
- Soluble and insoluble raw materials show different patterns of nanoparticles.

Supplementary material

Supplementary Fig. S1. Examples of mathematical conversion of raw Span data curves into smooth curves using the Contonian frequency (*H*) – *Gelsemium*.
Supplementary Table S1. Examples of three-way ANOVA statistical analyses applied to the Span values obtained with NTA – *Gelsemium*.
Supplementary Table S2. Examples of three-way ANOVA statistical analyses applied to the Span values obtained with NTA – *Cuprum.*
Supplementary Table S3. Examples of two-way ANOVA statistical analyses applied to the Span values obtained with NTA – *Gelsemium.*
Supplementary Table S4. Examples of two-way ANOVA statistical analyses applied to the Span values obtained with NTA – *Cuprum.*
Supplementary Table S5. Examples of Contonian frequency (*H*) calculations – *Gelsemium*.
Supplementary Table S6. Examples of Contonian frequency (*H*) calculations – *Cuprum.*

Funding
This study was funded entirely by private donations.

Conflict of Interest
None declared.

Acknowledgement
This study was financed by private donations from patients and doctors, and by the support of the Unio Homoeopathica Belgica (Belgian Homeopathic Union of Doctors). PHARAHOM (Belgian Association of Homeopathic Pharmacists) financed the production process. We thank them all.

References

1 European Pharmacopoeia. (Ph.Eur.), 11th Edition. Council of Europe. European Directorate for the Quality of Medicines; 2021
2 Mathie RT, Lloyd SM, Legg LA, et al. Randomised placebo-controlled trials of individualised homeopathic treatment: systematic review and meta-analysis. Syst Rev 2014;3:142
3 Mathie RT, Van Wassenhoven M, Jacobs J, et al. Model validity of randomised placebo-controlled trials of individualised homeopathic treatment. Homeopathy 2015;104:164–169
4 Hamre HJ, Glockmann A, von Ammon K, Riley DS, Kiene H. Efficacy of homoeopathic treatment: systematic review of meta-analyses of randomised placebo-controlled homoeopathy trials for any indication. Syst Rev 2023;12:191
5 Rutten L, Mathie RT, Fisher P, Goossens M, van Wassenhoven M. Plausibility and evidence: the case of homeopathy. Med Health Care Philos 2013;16:525–532

6 Klein SD, Würtenberger S, Wolf U, Baumgartner S, Tournier A. Physicochemical investigations of homeopathic preparations: a systematic review and bibliometric analysis—Part 1. J Altern Complement Med 2018;24:409–421
7 Tournier A, Klein SD, Würtenberger S, Wolf U, Baumgartner S. Physicochemical investigations of homeopathic preparations: a systematic review and bibliometric analysis—Part 2. J Altern Complement Med 2019;25:890–901
8 Tournier A, Würtenberger S, Klein SD, Baumgartner S. Physicochemical investigations of homeopathic preparations: a systematic review and bibliometric analysis—Part 3. J Altern Complement Med 2021;27:45–57
9 Demangeat JL. Water proton NMR relaxation revisited: ultrahighly diluted aqueous solutions beyond Avogadro's limit prepared by iterative centesimal dilution under shaking cannot be considered as pure solvent. J Mol Liq 2022;360:119500
10 Van Wassenhoven M, Goyens M, Henry M, Cumps J, Devos P. Verification of nuclear magnetic resonance of traditional homeopathically manufactured metal (*Cuprum metallicum*) and plant (*Gelsemium sempervirens*) medicines and controls. Homeopathy 2021;110:42–51
11 Esposito F, Wolf U, Baumgartner S. NMR relaxation time investigation of highly diluted aqueous solutions of silica-lactose. J Mol Liq 2021;227:115975
12 Van Wassenhoven M, Goyens M, Henry M, Capieaux E, Devos P. Nuclear Magnetic Resonance characterization of traditional homeopathically manufactured copper (*Cuprum metallicum*) and plant (*Gelsemium sempervirens*) medicines and controls. Homeopathy 2017;106:223–239
13 Demangeat JL. Gas nanobubbles and aqueous nanostructures: the crucial role of dynamization. Homeopathy 2015;104:101–115
14 Demangeat JL. NMR relaxation evidence for solute-induced nanosized superstructures in ultramolecular aqueous dilutions of silica-lactose. J Mol Liq 2010;155:71–79
15 Tiezzi E, Catalucci M, Marchetti N. The supramolecular structure of water. Int J Des Nat Ecodyn 2010;5:10–20
16 Baumgartner S, Wolf M, Skrabal P, et al. High-field 1H T(1) and T (2) NMR relaxation time measurements of H_2O in homeopathic preparations of quartz, sulfur, and copper sulfate. Naturwissenschaften 2009;96:1079–1089
17 Demangeat JL. NMR water proton relaxation in unheated and heated ultrahigh aqueous dilutions of histamine: evidence for an air-dependent supramolecular organisation of water. J Mol Liq 2009;144:32–39
18 Demangeat JL, Gries P, Poitevin P, et al. Low-field NMR water proton longitudinal relaxation in ultrahighly diluted aqueous solutions of silica-lactose prepared in glass material for pharmaceutical use. Appl Magn Reson 2004;26:465–481
19 Tiezzi E. NMR evidence of a supramolecular structure of water. Ann Chim 2003;93:471–476
20 Chikramane PS, Suresh AK, Bellare JR, Kane SG. Extreme homeopathic dilutions retain starting materials: a nanoparticulate perspective. Homeopathy 2010;99:231–242
21 Van Wassenhoven M, Goyens M, Dorfman P, Devos P. Particle characterisation of traditional homeopathically manufactured medicine *Cuprum metallicum* and controls. Int J High Dilution Res 2021;20:11–28
22 Dei A. Experimental evidence supports new perspectives in homeopathy. Homeopathy 2020;109:256–260
23 Van Wassenhoven M, Goyens M, Capieaux E, Devos P, Dorfman P. Nanoparticle characterisation of traditional homeopathically manufactured *Cuprum metallicum* and *Gelsemium sempervirens* medicines and controls. Homeopathy 2018;107:244–263
24 Temgire MK, Suresh AK, Kane SG, Bellare JR. Establishing the interfacial nano-structure and elemental composition of homeopathic medicines based on inorganic salts: a scientific approach. Homeopathy 2016;105:160–172
25 Montagnier L, Aïssa J, Ferris S, Montagnier JL, Lavallée C. Electromagnetic signals are produced by aqueous nanostructures derived from bacterial DNA sequences. Interdiscip Sci 2009;1:81–90
26 Bell IR, Muralidharan S, Schwartz GE. Nanoparticle characterisation of traditional homeopathically manufactured silver (*Argentum metallicum*) medicines and placebo controls. J Nanomed Nanotechnol 2015;6:1000311
27 Konovalov AL, Ryzhkina LS. Formation of nanoassociates as a key to understanding of physicochemical and biological properties of highly dilute aqueous solutions. Russ Chem Bull 2014;63:1–14
28 Elia V, Ausanio G, Gentile F, Germano R, Napoli E, Niccoli M. Experimental evidence of stable water nanostructures in extremely dilute solutions, at standard pressure and temperature. Homeopathy 2014;103:44–50
29 Duval E, Adichtchev S, Sirotkin S, Mermet A. Long-lived submicrometric bubbles in very diluted alkali halide water solutions. Phys Chem Chem Phys 2012;14:4125–4132
30 Chikramane PS, Kalita D, Suresh AK, Kane SG, Bellare JR. Why extreme dilutions reach non-zero asymptotes: a nanoparticulate hypothesis based on froth flotation. Langmuir 2012;28:15864–15875
31 Ives JA, Moffett JR, Arun P, et al. Enzyme stabilization by glass-derived silicates in glass-exposed aqueous solutions. Homeopathy 2010;99:15–24
32 Rajendran ES. Nanomaterial characterization of diluted *Platina* and alcohol control samples. Homeopathy 2023;112:144–151
33 Cartwright SJ. Solvatochromic dyes detect the presence of homeopathic potencies. Homeopathy 2016;105:55–65
34 Cartwright SJ. Interaction of homeopathic potencies with the water soluble solvatochromic dye bis-dimethylaminofuchsone. Part 1: pH studies. Homeopathy 2017;106:37–46
35 Demangeat JL. Towards a rational insight into the paradox of homeopathy. Adv Complement Altern Med 2018;2:121–133
36 Malm AV, Corbett JCW. Improved Dynamic Light Scattering using an adaptive and statistically driven time resolved treatment of correlation data. Sci Rep 2019;9:13519
37 Kestens V, Bozatzidis V, De Temmerman PJ, Ramaye Y, Roebben G. Validation of a particle tracking analysis method for the size determination of nano- and microparticles. J Nanopart Res 2017;19:271
38 Kikuchi K, Takeda H, Rabolt B, et al. Hydrogen particles and supersaturation in alkaline water from an alkali–ion–water electrolyzer. J Electroanal Chem (Lausanne) 2001;506:22–27
39 Otsuka I. Effect of 1:2 aqueous dilution on O_2 nanobubbles in a 0.1 M Na_2CO_3 solution. Proc 59th Annual Meeting International Society of Electrochemistry. September 7th–12th, 2008, Seville, Spain; 139
40 Nirmalkar N, Pacek AW, Barigou M. On the existence and stability of bulk nanobubbles. Langmuir 2018;34:10964–10973
41 Peck R, Olsen C, Devore JL. Introduction to Statistics and Data Analysis. 3rd ed. Cengage Learning
42 Conte RR, Berliocchi H, Lasne Y, Vernot G. Théorie des hautes dilutions et aspects expérimentaux. Ed Polytechnica ISBN 2-84054-046-0
43 Van Wassenhoven M, Nysten B, Goyens M, Dorfman P, Devos P, Magnin D. The ion partition detected in homeopathically manufactured medicine *Cuprum metallicum* and controls. Int J High Dilution Res 2022;21:67–84
44 Pegram LM, Record MT Jr. Hofmeister salt effects on surface tension arise from partitioning of anions and cations between bulk water and the air-water interface. J Phys Chem B 2007;111:5411–5417
45 Zhang XH, Wu ZH, Zhang XD, Li G, Hu J. Nanobubbles at the interface of HOPG and ethanol solution. Int J Nanosci 2005;4:399–407 and Errata Int J Nanosci 2010;9:383–384
46 Jin F, Ye J, Hong L, Lam H, Wu C. Slow relaxation mode in mixtures of water and organic molecules: supramolecular structures or nanobubbles? J Phys Chem B 2007;111:2255–2261

47 Alheshibri M, Craig VSJ. Differentiating between nanoparticles and nanobubbles by evaluation of the compressibility and density of nanoparticles. J Phys Chem 2018;122:21998–22007
48 Alheshibri M, Craig VSJ. Generation of nanoparticles upon mixing ethanol and water; Nanobubbles or Not? J Colloid Interface Sci 2019;542:136–143
49 Hampton MA, Nguyen AV. Nanobubbles and the nanobubble bridging capillary force. Adv Colloid Interface Sci 2010;154:30–55
50 Thormann E, Simonsen AC, Hansen PL, Mouritsen OG. Force trace hysteresis and temperature dependence of bridging nanobubble induced forces between hydrophobic surfaces. ACS Nano 2008; 2:1817–1824
51 Bunkin NF, Yurchenko SO, Suyazov NV, Shkirin AV. Structure of the nanobubble clusters of dissolved air in liquid media. J Biol Phys 2012;38:121–152
52 Jin F, Ye X, Wu C. Observation of kinetic and structural scalings during slow coalescence of nanobubbles in an aqueous solution. J Phys Chem B 2007;111:13143–13146
53 Fisher P. Homeopathy and intellectual honesty. Homeopathy 2017;106:191–193
54 Agarwal A, Ng WJ, Liu Y. Principle and applications of microbubble and nanobubble technology for water treatment. Chemosphere 2011;84:1175–1180
55 Eklund F, Swenson J. Stable air nanobubbles in water: the importance of organic contaminants. Langmuir 2018;34; 11003–11009
56 Sedlák M, Rak D. Large-scale inhomogeneities in solutions of low molar mass compounds and mixtures of liquids: supramolecular structures or nanobubbles? J Phys Chem B 2013;117; 2495–2504
57 Upadhyay RP, Nayak C. Homeopathy emerging as nanomedicine. Int J High Dilution Res 2011;10:299–310
58 Ullman D. Exploring possible mechanisms of hormesis and homeopathy in the light of nanopharmacology and ultra-high dilutions. Dose Response 2021;19:15593258211022983

